

Supramolecular interfacial architectures for biosensing

Fang Yu ¹, Danfeng Yao ¹, Danica Christensen ¹, Thomas Neumann ², Eva-Kathrin Sinner ³,
Wolfgang Knoll ¹

¹ Max-Planck Institute for Polymer Research, Ackermannweg 10, Mainz, 55128, Germany

² Graffinity Pharmaceuticals AG, Im Neuenheimer Feld 518 - 519, 69120 Heidelberg, Germany

³ Max-Planck-Institute of Biochemistry, Am Klopferspitz 18A, 82152, Munich, Germany

ABSTRACT

This contribution summarizes some of our efforts in designing, assembling and functionally characterizing supramolecular interfacial architectures for bio-affinity studies and for biosensor development. All the surface interaction studies will be based on the recently introduced novel sensor platforms involving surface plasmon fluorescence spectroscopy (SPFS) and -microscopy (SPFM). Emphasis will be put on documenting the distance-dependence of fluorescence intensity at the metal-dielectric interface and utilizing this principle to optimize the conformation/orientation of the interfacial supra-molecular sensor coatings. This is exemplified by a number of examples, including a layer-by-layer assembly system, antibody-antigen interactions, oligonucleotide-oligonucleotide, and oligonucleotide-PCR amplicon hybridization. For practical sensing purposes, a three-dimensionally extended surface coating is then employed to overcome the fluorescence quenching problem on a planar matrix. A commercial dextran layer is shown to be an optimized matrix for SPFS, with an example of a protein-binding study.

1. INTRODUCTION

The biological functions of most macromolecules depend on their ability to interact with other molecules. While in the lab environment, haptens, tracers, immunoconjugates and antibodies are routinely characterized to determine their identities and purities, their kinetic and thermodynamic properties are seldomly acquired. Laborious experiments may be demanded for the determination of these parameters if applying conventional techniques. In this context, high performance biosensors have been developed. Generally speaking, biosensors are devices that combine the specificity of biological molecules with physical detection strategy, e.g., using optical or electronic systems. Specific bio-recognition elements are immobilized on the so-called transducer surface in order to detect the specific molecular interaction and convert this event into an electrochemical, optical, mass, thermal or other signal. ¹ In addition to their primary sensing tasks, biosensors have been increasingly impacting biomolecular interaction analysis (BIA). These technologies have proved to have greatly simplified the task of BIA with their easy access to high-quality kinetic and thermodynamic data of interfacial biomolecular interactions. Recently, even more exciting progress has been made to allow for large-scale interaction studies ² for the development of complete sets of genomic/proteomic interaction maps.

Apart from inventing better biosensing schemes by implanting novel ideas from physics, the design of a functional biological matrix on the transducer is one of the key issues toward realizing a successful biosensor. Generally speaking, an ideal matrix should at least meet the following requirements: (1) it has to expose an optimized density of highly selective and specific biofunctional groups for the recognition of the analyte molecule, (2) it has to suppress non-specific adsorption, (3) it should exhibit a robust chemistry against regeneration conditions, (4) and it should have minimal impact (i.e. 'matrix effect') on the bio-interactions. These criteria become more specific for each individual analyte of interest. For example, it is obviously true that a large/highly charged analyte demands more spacing between immobilized probe molecules. ^{3,4} In addition to that, each biosensor may define its own 'ideal matrix' due to the different physical principle it is based on. ^{5,6}

In this report, we will concentrate on introducing interfacial architectures that are properly designed for and involved in the sensing tasks of a new biosensing concept – surface plasmon fluorescence spectroscopy (SPFS) ⁷⁻¹⁰ which uses the

interfacial light of a surface plasmon mode to excite the fluorophores carried by analyte molecules at a metal-liquid interface. The emitted fluorescence photons are then monitored and analyzed to give information about the behavior of the analyte itself. Like the surface-enhanced Raman spectroscopies (SERS),¹¹ SPFS also takes advantage of the enormous field-enhancement of a surface plasmon wave which is responsible for the substantial sensitivity enhancement in bio-interaction studies. At the commonly used gold/water interface, the evanescent field of a surface plasmon is enhanced by a factor of ~ 18 (at $\lambda = 633$ nm) compared to the incident field at the respective resonance angle, and then decays exponentially into the dielectric medium, with a penetration depth of approx. $L_z = 150$ nm which defines SPFS' surface specificity. (cf. Figure 1)

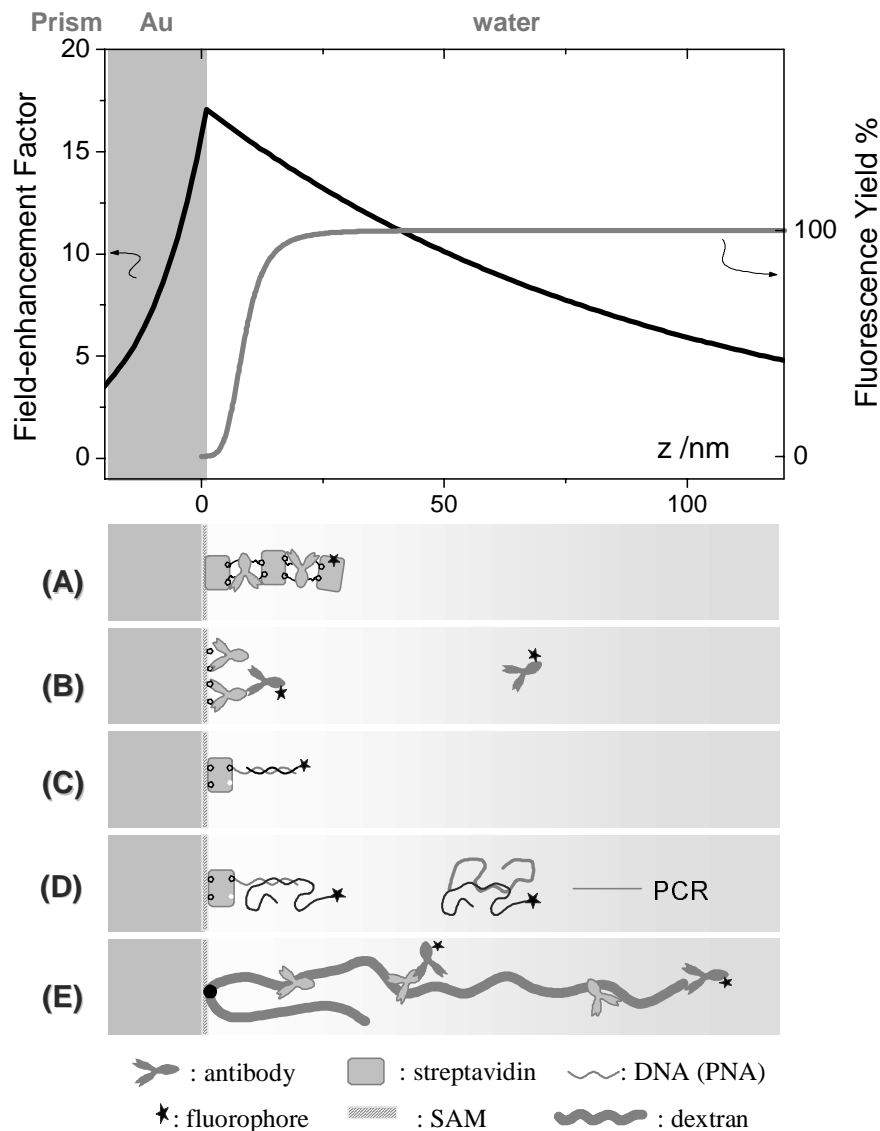


Figure 1. (Top panel) Intensity profile of a surface plasmon with the evanescent field extending into the dielectric medium (water) in contact with the metal (Au) layer (black line), and the fluorescence intensity profile of a fluorophore near a (quenching) metal surface (grey line). (A), (B), (C), (D), (E) Schematic cartoons of the interfacial architectures studied in this work: (A) A layer-by-layer assembly system based on biotin-SA interaction, (B) antibody bindings on a biotin SAM layer; (C) oligonucleotide hybridization based on a biotin SAM/streptavidin/DNA(or PNA) probe multi-layer architecture, and (D) PCR product hybridization based on a biotin SAM/streptavidin/PNA probe multi-layer architecture; (E) antibody-antigen interaction in a dextran matrix.

Within this several hundreds of nanometer thin liquid layer, the accumulation of the analyte molecules alters the optical properties of the interface and can be sensed by an angular shift in the surface plasmon resonance (SPR) minimum. If the analyte molecule carries a fluorescent dye, the dye will be excited and emit fluorescence. In this sense, SPFS can be considered as a combination tool, which simultaneously conveys the information of a local refractive index change and of the fluorophore concentration. By this, it offers the potential for a more detailed surface investigation than conventional SPR. For example, a recent report elucidated this application of SPFS in monitoring/distinguishing multi-component protein adsorption based on its dual signal sensing ability.¹²

As it is well known, the fluorescence yield of fluorophores near a metal exhibits a highly pronounced distance-dependent behavior.^{7,13} Briefly, within a short separation distance range (approx. 20-30 nm), the fluorescence of the fluorophores can be 'quenched' by a Förster energy transfer mechanism or, can be 'back-coupled' via the plasmon coupling device as red-shifted re-radiation. Both effects reduce the effective fluorescence emission. Beyond this range, as the distance increases further, the fluorescence yield weakens with the fading of the evanescent field. On the one hand, this strong distance dependence of the fluorescence causes problems in the quantification of the surface analyte, whose fluorescence yield may depend on its unpredictable position/orientation at the surface. On the other hand, it results in a much more pronounced distance information than the surface plasmon evanescent field ($L_z = \sim 150$ nm), which may offer a clearer understanding of the three-dimensional distribution of the bound molecules. Obviously, a planar functional surface (or two-dimensional surface) is experimentally desirable for pronouncing such a distance effect. Combining the 2D surface with the layer-by-layer assembly technique, a distance profile of the fluorescence yield on SPFS has been determined.¹⁴ In this study, 2D model systems were fabricated by (mixed) self-assembled monolayers (SAMs) on a gold surface, exposing a functional ligand (e.g., biotin) with controllable density. Based on the SAM layer, antibodies (e.g., anti-biotin antibodies, cf. Figure 1(B)) can be immobilized via immuno-interaction, or tetrameric streptavidin can be coupled to mediate a subsequent functionalizations (e.g., via the biotinylated DNA/PNA probes, cf. Figure 1(C)(D), or a layer-by-layer system, cf. Figure 1(A)). In particular, streptavidin is used to generate a DNA (PNA) probe matrix for the following reasons. Firstly, streptavidin symmetrically possesses four biotin binding sites, leaving at least one of them for the following binding of biotinylated probe molecules. Secondly, the affinity between biotin and streptavidin is extremely high and could be further enhanced by the potential multiple attachment to the surface-confined biotin moieties, enabling a robust sensing surface. Thirdly, streptavidin is slightly negatively charged at physiological pH, which eliminates non-specific adsorption of DNA molecules via electrostatic interaction. Fourthly, the dimension and the limited binding pockets of streptavidin define a certain probe density, which has proved to be highly efficient for target hybridization. Finally, the biotin-streptavidin matrix additionally separates the fluorescently labeled molecules from the metal surface by at least 6 nm owing to the thickness of the biotinylated SAM (~ 1.6 nm) and the dimension of the streptavidin molecule (5.6 nm \times 4.2 nm \times 4.2 nm, as determined by X-ray diffraction). Therefore, the metal induced fluorescence quenching can be reduced to some extent.

On the other hand, a spatially extended three-dimensional matrix meets the demand for realizing reliable SPFS sensing in almost every aspect. Firstly, the fluorescence emission from the fluorophores can be integrated at different distances from the sensor surface; therefore the distance behavior of fluorescence is averaged. Secondly, the interaction layer can be displaced from the metal considering the large steric hindrance at the tethering point of the brush backbone. Thirdly, the larger volume of the matrix offers a larger molecular retention, which leads to an effective increase of the binding site density available for the analyte to bind to and favors sensitive detection, as has been clearly indicated by the sensitivity increase in a label-free SPR analysis¹⁵. Coincidentally, we found that the dextran matrix from Biacore AB was an excellent 3D platform for proving the principle of SPFS with an immuno-interaction model system. (cf. Figure 1(E))

In the following, we start with various examples of protein/oligonucleotide interactions on 2D functional matrices. The distance-dependent fluorescence is demonstrated and in return used to depict the interfacial architectures of bound protein/ oligonucleotide. Particularly, a label-free detection mode of SPFS will be proposed taking advantage of the stretching-upon-hybridization mechanism of the fluorescently tagged probe oligonucleotide. Then, the distance profile of fluorescence will be used to understand the conformation of hybridized PCR products at various ionic strengths. The last set of example that we present concerns a protein sensing based on a 3D matrix. We will demonstrate the elimination of the distance-dependent fluorescence and a great enhancement of the detection sensitivity with the aid of the 3D dextran layer.

2. EXPERIMENTAL

2.1 Instrumental

A surface plasmon fluorescence spectroscopy (SPFS) setup is schematically depicted in Figure 2. The beam of a HeNe laser (Uniphase, 5 mW, $\lambda = 632.8$ nm) passes through a chopper that is connected to a lock-in amplifier (EG&G). The modulated beam then passes through two polarizers (Glan-Thompson), by which the intensity and the plane of polarization of the laser can be adjusted. A programmable shutter was installed to constantly block the laser (unless data points are recorded), thus minimizing the photo-bleaching effect of the fluorescent dyes. Next, the beam is reflected off the base of the coupling prism (Schott, LASFN9) and is focused by a lens ($f = 50$ mm, Owis) onto a photo-diode detector. The fluorescence emission of the sample is collected from the backside of the prism by another lens ($f = 50$ mm, Owis), and passes then through an interference filter ($\lambda = 670$ nm, $\Delta\lambda = 10$ nm, LOT, 80% transmittance) into a photomultiplier tube (PMT, Hamamatsu), which is connected to a photon-counter (Agilent) unit. The fluorescence detection unit is mounted on the goniometer rotating together with the prism (sample) at θ , while the photo-diode detecting the reflected light rotates at 2θ . Data acquisition and control of the system electronics are accomplished by custom programs. A home-built glass flow-cell was equipped to efficiently deliver the sample liquid, and reduce the mass-transport rate of analyte to the interface, by running at a flow-rate of 3 mL/min.

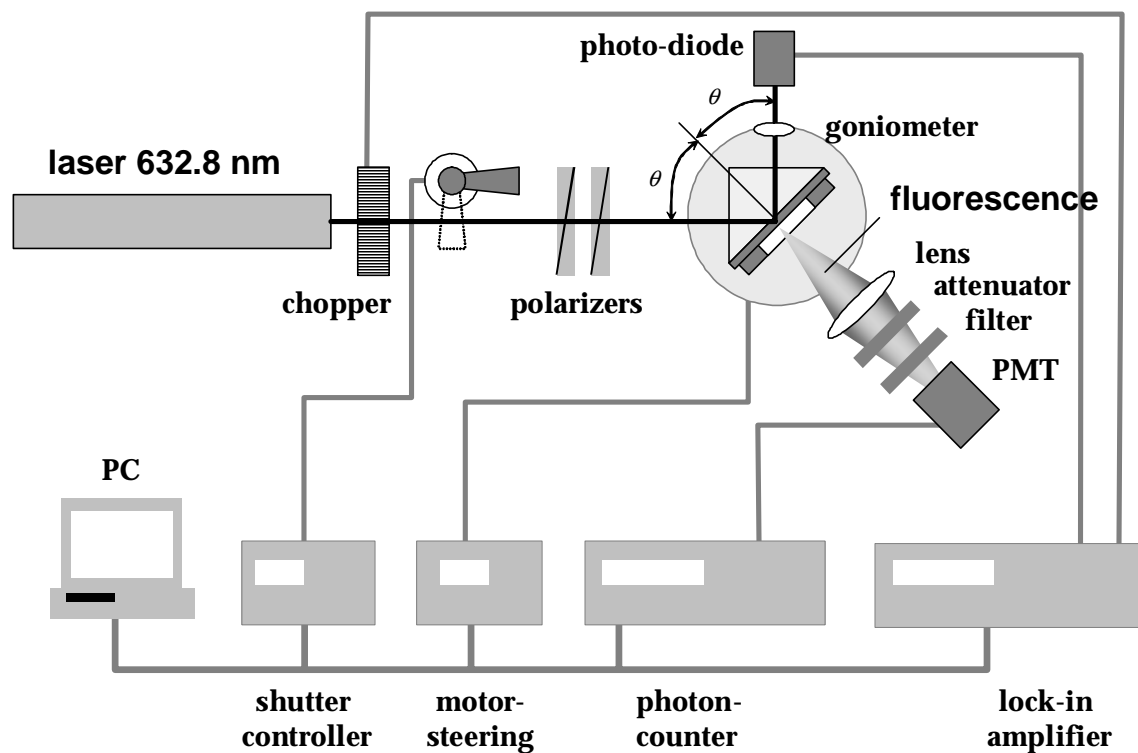


Figure 2. Schematic experimental setup for surface plasmon fluorescence spectroscopy in a Kretschmann configuration.

2.2 Materials and sample preparation

Here, for 2D systems, we routinely firstly covered the golden sensor surface with a SAM. The SAM was composed of a mixture of biotinylated thiol (Biotinamino-capronacid-amidodioctyl-mercaptopropionamid, functional thiol) and an OH-terminated alkyl-thiol (2-Mercaptopropionacid-[2-(2-hydroxyethoxy)] ethylamid, spacer thiol) (cf. Table 1), with a well engineered ratio of 1:9 for maximizing the subsequent streptavidin binding amount. The thiols and the streptavidin were obtained from Roche Diagnostics.

The anti-biotin mouse monoclonal antibody 2F5 (isotype IgG 1.k), the Alexa Fluor 647 labeled rabbit anti-mouse IgG (abbreviated as AF-RaM, reacts with the IgG heavy chains and all classes of Ig light chains from mouse, dye-to-IgG ratio: 4.8), Alexa Fluor (AF) 647 labeled streptavidin (abbreviated as AF-SA, dye-to-SA ratio: 4.3), the biotinylated goat-anti-mouse IgG (abbreviated as B-GaM, biotin-to-IgG ratio 5.8), and the AF 647 monoclonal antibody labeling kit were purchased from Molecular Probes. The 2F5 antibody was labeled with AF 647 dye by following a standard protocol. The dye-to-protein ratio was 4.4, determined spectrophotometrically by measuring the adsorbance at $\lambda=647$ nm (AF 647) and $\lambda=278$ nm (antibody) in PBS buffer.

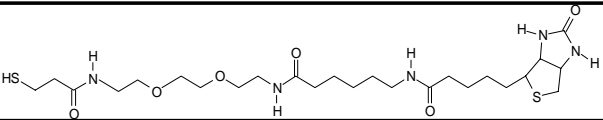
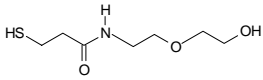
Biotin thiol	
Spacer thiol	
BioCy5T15	5'-biotin-(TTT) ₅ -TGT ACA TCA CAA CTA -Cy5 -3'
PNA P2	biotin-(eg) ₉ -TGT ACA TCA CAA CTA-COOH
PNA P2-3	NH ₂ -TGT ACA TCA CAA CTA- (eg) ₉ -biotin
T0	5'-TAG TTG <u>T</u> CA <u>C</u> GT ACA-3'
T1	5'-TAG TTG TGA <u>C</u> GT ACA-3'
T2	5'-TAG TTG TGA TGT ACA-3'
Cy5-T2	5'-Cy5-TAG TTG TGA TGT ACA-3'
Cy5-T75	5'-Cy5-(TTT) ₁₀ -TAG TTG TGA TGT ACA- (TTT) ₁₀ -3'
Cy5-Mu-196 (sense strand)	5'- Cy5 -... ... TAG TTG TGA TGT ACA -3'

Table 1. Thiols and DNA sequences used in this study.

The biotinylated Cy5 labeled DNA probe (BioCy5T15) and DNA targets (T0, T1, T2, Cy5-T2, Cy5-T75) were purchased from MWG-biotech, and are listed in Table 1. A poly-T (15-mer) spacer was designed in the probe to reduce the steric hindrance of surface hybridization. The biotinylated PNA P2 and PNA P2-3 are synthesized in our group. Ethylene glycol (eg) spacers were designed in PNA probes. The 75-mer target T75 consists of the same recognition sequences as the 15-mer target T2, however, has two flanks of poly T (30-mer). T2 and T75 were fully complementary to the probe, i.e., they define a mismatch zero (MM0) situation, while one-base mismatch (MM1) was designed in the sequences of T1. A two-base mismatch (MM2) was designed for the T0 target.

Plasmid TOPO 2.1 was used as the template for PCR amplification. The Cy5 labeled forward and reverse primers were purchased from MWG-Biotech. Reagents for each 50 μ L reaction included: 5 units of Taq polymerase (Amersham Biosciences), 1 \times PCR buffer (Amersham Biosciences), 60 pmol of the forward primer and 80 pmol of reverse primer (MWG-Biotech), 0.2 mM dNTPs (Fermentas) and 100 ng of the plasmid. After an initial denaturation step at 96°C for 1 min, each of the 30 cycles of amplification consisted of 30 s of template denaturation at 96°C, 30 s of primer annealing at 50°C and 30 s of primer extension at 72°C. The resulting 196 bp PCR product (Cy5-Mu-196) was identified by agarose electrophoresis (2%). Ethanol precipitation was performed afterwards in order to remove the salts, dNTPs, excess primers and enzyme from the PCR sample. For 50 μ l of PCR sample, 125 μ l ethanol and 5 μ l of sodium acetate (3 M) were added. The mixture was shaken, and then kept at -20°C for more than 6 hours to induce precipitation. The PCR products were collected by centrifugation at 16, 000 g for ~0.5 hours. The concentration of PCR product could be

determined by reading the adsorption of Cy5 at $\lambda=650$ nm. The PCR products underwent the following denaturation process prior to the biosensing studies, unless otherwise stated: the heat denaturation was composed of three steps, heating the DNA sample (in 10 mM PB buffer) at 96°C for 10 min, quickly quenching it to 0°C in an ice-water mixture and returning to room temperature.

N-ethyl-N'-(3-dimethylaminopropyl) carbodiimide hydrochloride (EDC) and N-hydroxysuccinimide (NHS) ethanolamine hydrochloride, ethanolamine, Sensor Chips CM5 without the plastic cartridge, Amine Coupling Kit, HBS-EP buffer (degassed 10 mM HEPES buffer saline, pH 7.4, 150 mM NaCl, 3 mM EDTA, 0.005% (v/v) surfactant P-20), Acetate 5.0 buffer (10 mM, pH 5.0), glycine buffer (10 mM, pH 1.7), carboxymethyl-dextran were obtained from Biacore AB (Uppsala, Sweden). In chapter 3.1, 3.6 and 3.7, a protocol based on EDC/NHS chemistry was used to covalently attach the streptavidin and IgG.¹⁶ A fraction of the carboxyl groups on the carboxyl SAM surface and dextran matrix were activated to form reactive N-hydroxysuccinimide esters using a solution of 0.2 M EDC and 0.05 M NHS in water. After this activation, 20 $\mu\text{g/mL}$ AF-SA or IgG prepared in sodium acetate, pH 5.0, was immobilized via the reaction of its nucleophilic groups. Afterwards, excess esters were deactivated using 1 M ethanolamine hydrochloride adjusted to pH 8.5 with sodium hydroxide, which also desalted loosely bound protein.

3. RESULTS AND DISCUSSIONS

3.1 A layer-by-layer assembly system

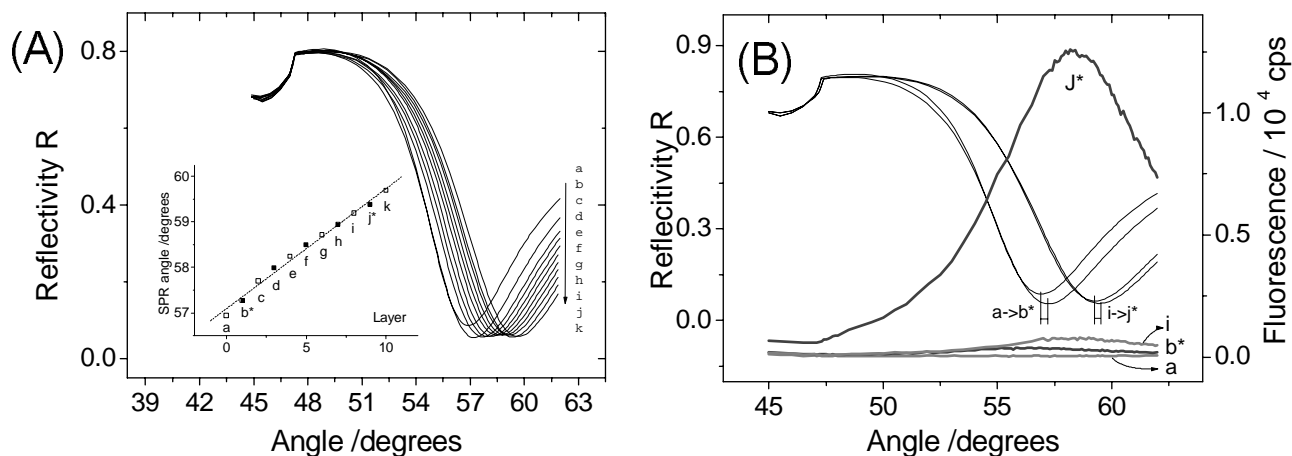


Figure 3: A layer-by-layer model built by alternating biotin-IgG and (labeled) streptavidin. (A) Angular SPR curves of each layer. The inset shows the SPR minimum position as a function of layer number. (B) SPR/fluorescence angular scans for layer 'a', 'b*', 'i' and 'j*'. Fluorescence was attenuated by a 2db neutral filter.

As the first example, we present a layer-by-layer (LbL) system that enables us to test the distance-dependent fluorescence at the metal surface. Apart from the electrostatic interaction, the most common application strategy for the LbL technique, biological affinity can also be used to deposit proteins by means of, e.g., the antigen-antibody interaction, biotin-avidin interaction, or the sugar-lectin interactions. The LbL techniques offer a way to control the separation distance between the molecules of interest to the base surface, which is of particular interest for investigating the distance behavior of the fluorescence yield by SPFS. In the following, we choose streptavidin and biotinylated IgG as the alternating molecules, a strategy reported previously.¹⁷ The layers can be selectively decorated by applying dye-labeled streptavidin.

A surface coated with a self-assembled monolayer of 3-mercaptopropionic-acid, was used for the covalent attachment of AF-SA by means of active ester chemistry. This reaction induced a SPR minimum shift of $\sim +0.27$ degrees and contributed a fluorescence intensity of $\Delta f \sim 350$ cps from peak to peak, shown in Figure 3(B) as curve b*. Subsequently,

the binding of biotin-GaM and SA from 20 $\mu\text{g}/\text{mL}$ solutions in HBS buffer were alternated. Plotting the SPR minimum shift of each layer versus the layer number (cf. Figure 3(A)), we can see a linear correlation, which means the layers were consistently built up without any sign of receding up to 10 layers. A linear fit yielded a slope of ~ 0.26 degree/layer, corresponding to a thickness slope of ~ 2 nm/layer, if assuming a refractive index of $n=1.45$ for both streptavidin and biotin-GaM.

On top of the 8th layer (a biotin-IgG layer) or the 4th double layer, i.e., at a distance of ~ 16 nm to the Au surface, another AF-SA layer was built, yielding a much stronger fluorescence signal of $\Delta f \sim 12000$ cps, which compares drastically to the fluorescence yield from the first AF-SA layer, by a factor of ~ 34 . This gives the intensity difference between quenched and un-quenched fluorescence molecules and strongly suggests the need of a decent spacing layer for the fluorescence molecules for real sensing applications. Also interesting is, that the fluorescence peak from the 1st AF-SA layer increased from ~ 400 cps to ~ 750 cps, after building up 7 bare protein layers. Two possibilities could be envisioned: 1) the effect is due to a conformational change of the 1st layer of AF-SA induced by subsequent layers on top of it; 2) a re-distribution of the surface plasmon electro-magnetic field due to the local refractive index altered by the subsequent dielectric layers.

3.2 Interfacial arrangement of antibodies

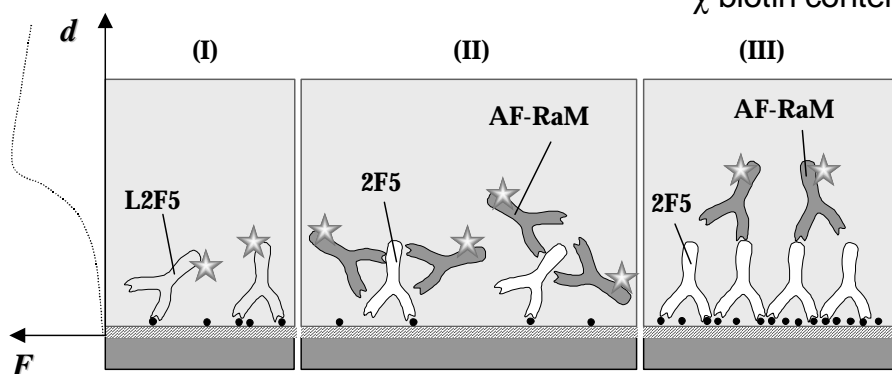
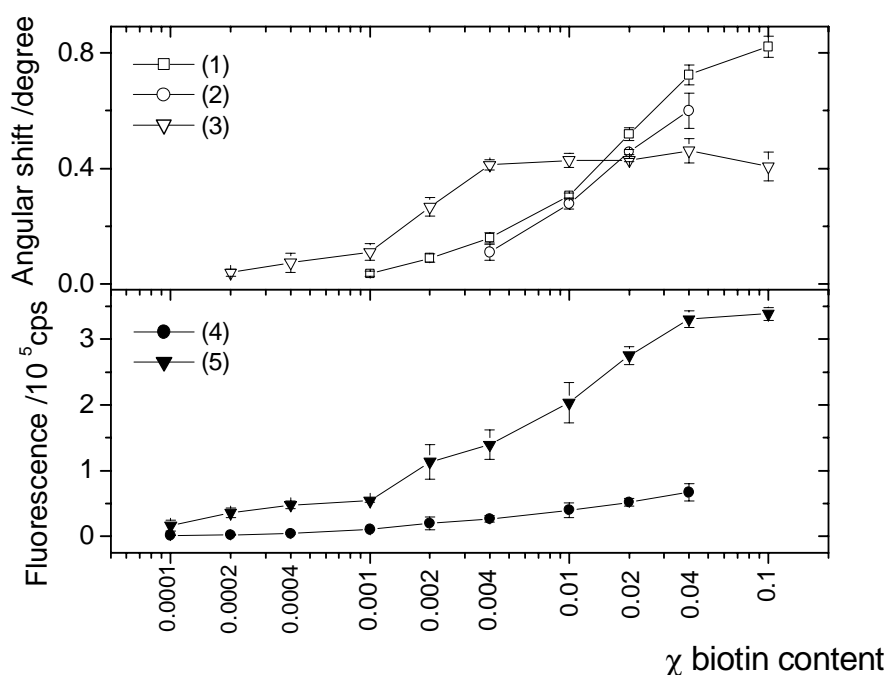


Figure 4 (A) End-point results of antibody bindings on biotin SAMs. (1) SPR of 2F5, (2) SPR of AF-2F5, (3) SPR of AF-RaM, (4) fluorescence of AF-2F5, (5) fluorescence of AF-RaM. (B) Schematics of the interfacial molecular architectures of (I) AF-2F5 binding, (II) 2F5 + AF-RaM binding on surfaces with lower biotin density and (III) 2F5 + AF-RaM binding on surfaces with higher biotin density. A drawing (F versus d) representing the distance dependent fluorescence yield above the gold/liquid interface is given on the left side.

In the second example, we will show how to utilize the distance information of the fluorescence signal to better understand the supramolecular arrangement of IgGs in fluorescence immunoassays.⁹ A series of Au surfaces with mixed biotin SAMs (biotin ratio $\chi = 0.1, 0.04, 0.02, 0.01, 0.004, 0.002, 0.001, 0.0004, 0.0002, 0.0001$, respectively) were prepared. Then the SPR/fluorescence signal of the directly binding labeled/unlabeled anti-biotin antibodies (2F5), as well as of the secondary antibody (AF-RaM) were recorded. Several interesting features emerged when plotting these end-point signals in Figure 4.

1) Comparing curve 1 with curve 3, one can see that the stoichiometric ratio of AF-RaM to 2F5 reversed at a critical biotin density, $\chi = 0.014$. This is due to the fact that AF-RaM reacts with all parts of mouse IgG in a rather nonspecific way. At a lower primary antibody density (cf. model (II) in Figure 4), the ample space in between the surface-antigens can accommodate more AF-RaM. As the packing density of 2F5 increases, the room shrinks and the neighboring molecules start to mutually block each other's epitopes. Thus, we see a largely reduced AF-RaM/2F5 ratio (cf. Figure 4 (III)) while the net amount of AF-RaM remained almost constant because of the increased number of 2F5. This steric effect can be similarly seen in the mixed SAM system where densely packed biotin thiols even reduces the net amount of SA binding.¹⁸

2) The AF-RaM yielded a much stronger fluorescence intensity compared to AF-2F5 (cf. curve 4 and curve 5), calibrated by their corresponding SPR signal. This can be easily explained by the metal-induced fluorescence quenching, since the primary antibody contacts with the metal more directly than the secondary antibody.

3) The fluorescence intensity did not scale linearly with the SPR signal among the AF-RaM data points (cf. curve 3 and curve 5). At a lower 2F5 density, there is enough space around each primary antibody, allowing for a 'lateral approach' of several AF-RaMs. While as the density of 2F5 increases, the AF-RaM tends to be pushed away from the gold and gets less quenched.

We demonstrated that SPFS offers more signal channels than mere SPR or mere fluorescence spectroscopy for understanding the molecular arrangement at the interface. However, the current labeling technique limited the resolution of having distance information, because it does not provide a site-specific control about the labeling position. Consequently, the distance information could be convoluted by the random distribution of dyes on a 15-20 nm large antibody molecule.¹⁹ Referring to the reports that it is possible to accurately position the dye by site-specific labeling or genetic engineering, we expect a more promising application of SPFS in understanding interfacial protein arrangement.

3.3 Stretching-upon-hybridization of oligonucleotide

In comparison with the protein system, labeling DNA at the designed end is commercially feasible. As a result, DNA's conformational change is expected to sensitively change the fluorescence intensity. Based on that, we will introduce a novel label-free DNA detection mode.

Firstly, biotinylated fluorescently labeled probes (BioCy5T15) was immobilized on a SA pre-coated surface, leading to a stable fluorescence signal baseline due to the high affinity of Biotin-SA interaction (data not shown). Following the preparation of the probe layer, hybridization kinetics with unlabeled MM0, MM1 and MM2 target sequences were recorded by SPFS at a 1 μM target concentration. After equilibrium was reached, the flow cell was rinsed by pure PBS buffer in order to desorb the hybridized strands from the surface. As presented in Figure 5(B), the specific hybridization by MM0 targets induced a significant increase of the probe fluorescence intensity. Based on the knowledge that a stiff helical part is formed in the hybridized duplex, we infer that the distance of the dye to the metal was increased with the stiff part orienting normal to the surface (cf. Figure 5(A)). Furthermore, we can see that the hybridization kinetics of MM0, MM1 and MM2 targets could be quantitatively distinguished. While in the case of two mismatching base pairs in the target no significant signal could be detected, a clear increase of fluorescence was seen during the binding of the MM1 and MM0 targets. The kinetic results are quite similar to the previously reported results with labeled targets.⁸

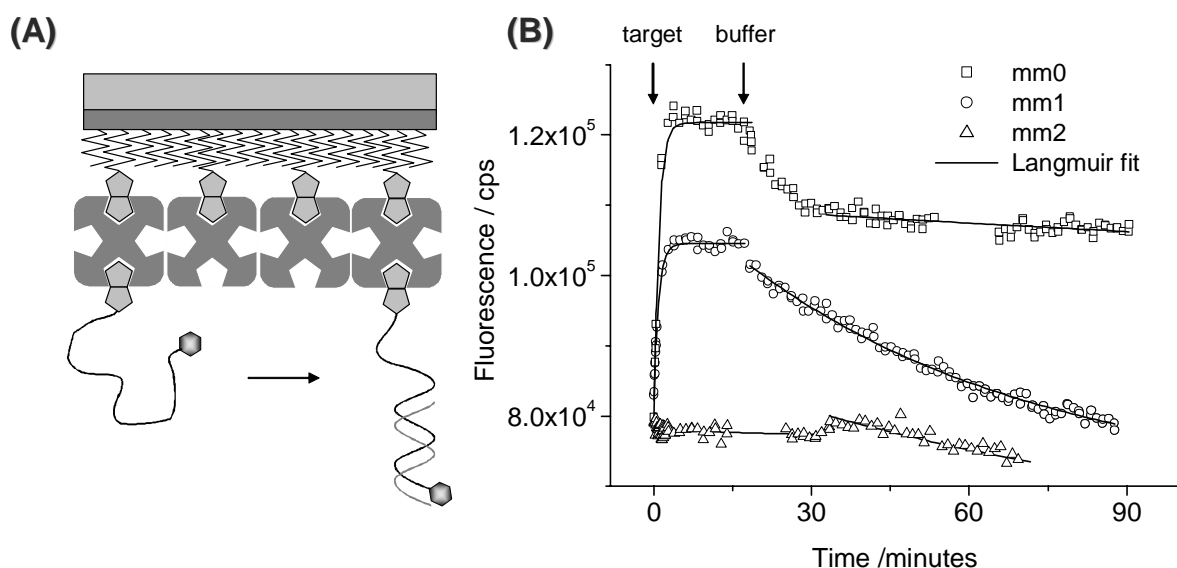


Figure 5: (A) Schematics of the conformational change of the biotinylated Cy5 labeled probe upon hybridization of unlabeled target and formation of a stiff helical structure in the duplex. (B) Hybridization kinetics of unlabeled targets to the labeled probe BioCy5T15 together with Langmuir fits. For MM0 targets, $k_{on}=3.1 \times 10^4 \text{ M}^{-1}\text{s}^{-1}$, $k_{off}=1.2 \times 10^{-4} \text{ s}^{-1}$; for MM1 targets, $k_{on}=1.8 \times 10^4 \text{ M}^{-1}\text{s}^{-1}$, $k_{off}=3.5 \times 10^{-4} \text{ s}^{-1}$; for MM2, it was difficult to obtain any kinetic constant.

This detection approach shares the similar principle with the molecular beacon technique, while in our case the 2D Au surface serves as a universal quencher for most of fluorescent dyes. Like the beacon technique, it is demanded to design hairpin structures in the probe in order to enhance its structural contrast, hence the signal difference, before and after the hybridization. Also, a careful tuning of the probe length, number of spacer bases, etc., would be expected to optimize the detection sensitivity.

3.4 Influence of the dye position

In the previous example, we have shown that the fluorescence intensity is very sensitive to the conformation/orientation of the oligonucleotide on a 2D sensor surface. This is partially due to the relatively clear picture of the way that oligonucleotides bind to the surface. However, for long chain DNA, such as PCR products, the situation is quite different. The PNA P2-3 and the PNA P2 probe are two PNA oligomers that have identical sequences, but differ in the position of the biotin label and eg spacers. Both the biotin and eg are present at the N-terminal of PNA P2, but at the C-terminal of PNA P2-3. This positional change is considered to have little effect on the PNA immobilization owing to the extraordinarily high affinity of biotin / SA. Hybridization of a Cy5 labeled 15 mer DNA target (Cy-T15) and a Cy5 labeled PCR product (Cy5-Mu-196) were tested on both probe surfaces. Both of the two hybridizations essentially related to the same 15-base recognition, so ideally they exhibited identical hybridization efficiency. However, the result was a different position of the dyes carried by the target oligonucleotides, as shown in Figure 6(A) by a large difference in equilibrium fluorescence intensities of the two probes. Clearly, upon hybridization with a PNA P2-3 derivatized surface, the 5' end of T15-Cy5, hence the Cy5 dye, was 'buried' deeply into the DNA layer and was significantly quenched by Au. Testing the Cy5-Mu-196 with the same probe surfaces gave significantly different results. Figure 6(B) shows that the two hybridizations signals were much closer to each other. Note that in the PCR hybridization case, the 15-base recognition sequence appears in the middle of the sense strand and is quite far from the dye position. The long chain between the dye and the recognition site enables good freedom of the dye position, i.e. even in the 'inversed' hybridization case the dye attached at the 5' end can still be placed away from the surface. Furthermore, the structural complexity of the PCR chain also overrules the sharp orientation effect.

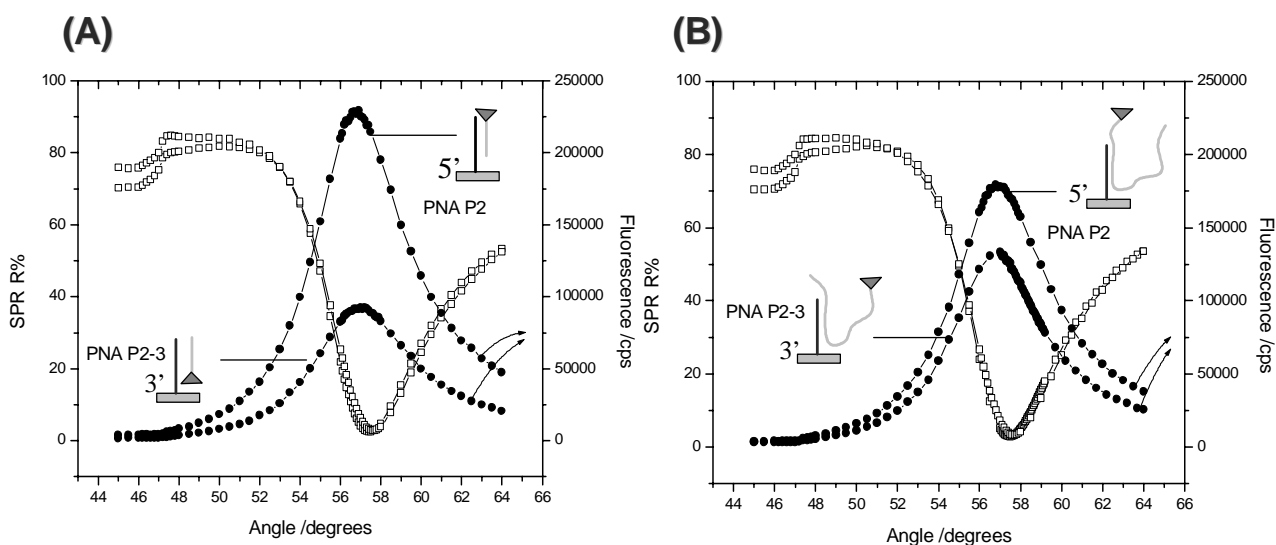


Figure 6: SPR/fluorescence angular scan curves at the equilibriums of hybridization of (A) Cy5-T75 and (B) Cy5-Mu-196 on PNA P2 and PNA P2-3 surfaces.

3.5 Stretching of oligonucleotide and PCR product in buffers of different ionic strength

In chapter 3.3, we have shown that hybridization can stretch the DNA backbone by forming a more rigid supra-molecular structure – a double helix. Considering that DNA is also a highly charged polyelectrolyte, we propose that the ionic strength can also vary the conformation of DNA, detected by the change in fluorescence intensity.

The experiments were performed in the following steps: A Cy5-labeled 75mer single-stranded oligonucleotide (Cy5-T75) or the previously used Cy5-Mu-196 were hybridized with a PNA P2 densely derivatized surface (ca. 4,000 Å² per strand) in a phosphate buffer with low ionic strength (10 mM Na⁺) (cf. Figure 7(A), (B)). Upon equilibrium, buffer (10 mM Na⁺) rinsing was started. Subsequently, buffers containing different Na⁺ concentrations varying from 50 mM to 1000 mM were sequentially applied in the rinsing phase. A corresponding stepwise fluorescence decrease was monitored. Upon switching the sodium concentration back to 10 mM, the fluorescence was partially recovered, and appeared on the prolongation of the desorption curve generated by the first rinsing with 10 mM Na⁺, which indicates little perturbation of the buffer switches to the target dissociation. Both targets showed identical behavior on densely immobilized PNA probe layers. The same experiments were performed on surfaces with a strategically reduced PNA P2 density (~40 times less than on the dense surface), by a so-called templated-immobilization method.²⁰ (cf. Figure 7(C), (D))

It is well known that the phosphate backbone of DNA is highly charged at low ionic strength condition (e.g. 10 mM Na⁺, pH 7.4). Therefore, the DNA strand tends to become more rigid and can stretch by electrostatic repulsion within one strand or between neighboring strands. Therefore, effective screening by counterions from the electrolyte solution lowers the electrostatic contribution to the inherent rigidity of the oligonucleotide and/or external repulsive force to the oligonucleotide and lowers its dye-to-metal distance. The argument was further strengthened by the result that the quantum yield of the fluorophore in solution was independent of the applied Na⁺ concentration range (data not shown). However, one can notice that the fluorescence remained nearly invariant in the range of sodium concentrations for Cy5-T75, but was still considerably dependent on the sodium concentration for Cy5-Mu-196. Since the probe dilution greatly increased the strand-to-strand distance, the vanishing of the ionic strength dependence of Cy5-T75 may suggest that the inter-strand repulsive force was the main contribution to its stretched conformation in low salt condition. In other words, the 75 mers were already collapsed on the surface in low salt condition, lacking the neighboring supporting force. On the other hand, the structural complexity of Cy5-Mu-196 helped to maintain its structural integrity on the surface without the help from neighboring strands, and made it still ionic strength responsive.

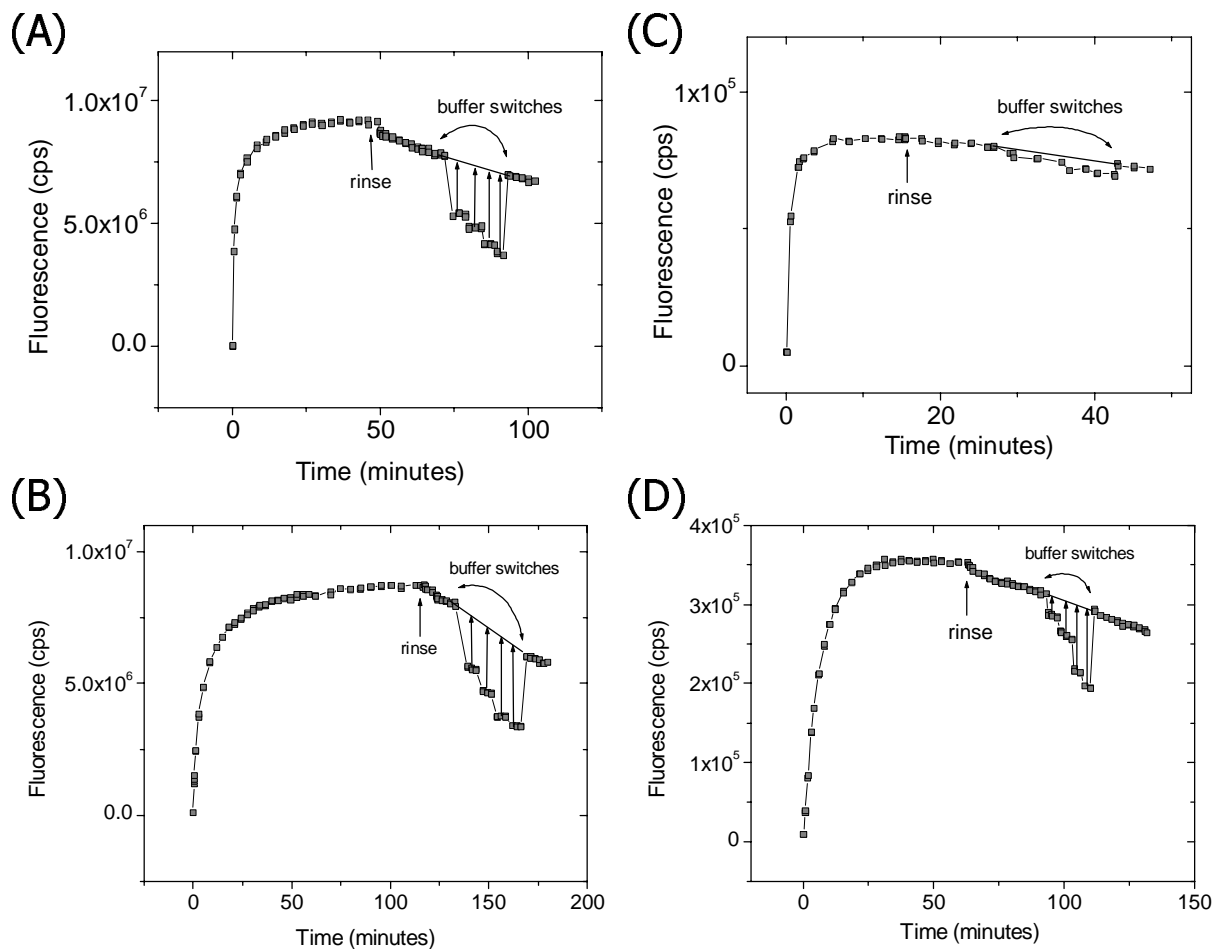


Figure 7: Na^+ concentration induced fluorescence variation demonstrated by the bound (A) Cy5-T75, (B) Cy5-Mu-196 on a densely immobilized PNA P2 surface (ca. $4,000 \text{ \AA}^2$ per strand), and the bound (C) Cy5-T75, (D) Cy5-Mu-196 on a diluted PNA P2 surface (ca. $160,000 \text{ \AA}^2$ per strand). 'Buffer switches' in the figures represents switching the phosphate buffers with 10 mM, 50 mM, 100 mM, 500 mM, 1000 mM Na^+ , sequentially.

3.6 Sensitivity demonstration on a 3D platform

Using the three-dimensional functional dextran matrix of the CM5 sensor chip of Biacore, the substrate (Au metal) induced fluorescence loss of bound fluorophores monitored by SPFS is expected to be largely reduced. Moreover, the distance-dependent fluorescence of the fluorophores located at different positions relative to the metal surface is convoluted to result in a coverage-independent fluorescence yield. This is then optimized for the limit of detection (LOD) assessment of SPFS. A simple one-to-one interaction model system is employed by covalently immobilizing mouse IgG to the carboxymethyl dextran matrix and by monitoring the AF-RaM binding from the bulk solution.

The range of the AF-RaM concentration used ensured a mass-transport limited binding behavior, which means the binding rate remains constant in the association phase and the rate is linearly dependent on the analyte concentration. A strictly linear dose-response curve is give in Figure 8(A) with a considerable mouse IgG loading amount (SPR angular shift = 1.33° , equivalent to $\sim 7 \text{ ng mm}^{-2}$). Three interesting features in the plot are noteworthy and are attributed to the use of the 3D dextran matrix: 1) the linear range of the curve spans over ~ 6 orders of magnitude; 2) the dose-response curve intersects with the baseline fluctuation level at $\sim 500 \text{ aM}$ ($5 \times 10^{-18} \text{ M}$); 3) the small error bar demonstrated the excellent reproducibility of the experiment and, thus, the precision of the analysis.

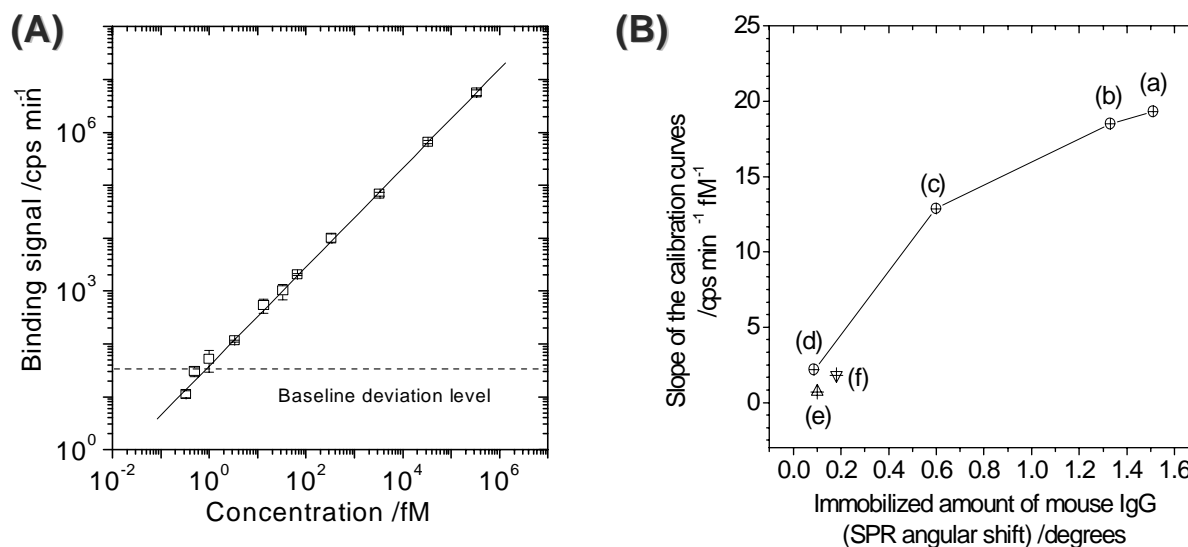


Figure 8: (A) Dose-response curve of AF-RaM binding to the mouse IgG immobilized dextran matrix (on CM5 chip). (B) Slopes of the dose-response curves versus the mouse IgG loading amount (quantified by SPR angular shift $\Delta\theta$). (a) CM5 chip, $\Delta\theta=1.51^\circ$, (b) CM5 chip, $\Delta\theta=1.33^\circ$, (c) CM5 chip, $\Delta\theta=0.61^\circ$, (d) CM5 chip, $\Delta\theta=0.088^\circ$, (e) LA chip, $\Delta\theta=0.18^\circ$, (f) LA chip, $\Delta\theta=0.09^\circ$.

An antigen-coverage dependence study was also conducted by controlling the contact time of mouse IgG with the activated NHS-ester groups in the dextran matrix (cf. chapter 2.2). The slopes of dose-response curves plotted against the immobilized mouse IgG amount are presented in Figure 8(B). Apparently the slopes of the dose-response curves, representing the binding probability of AF-RaM, are dependent on the mouse IgG amount on the chips. The curve that links these points deviates from a linear relation which can be explained by the following consideration. Firstly, the epitopes are mutually blocked at high surface antigen density, leading to a decrease of the recognition site number. Secondly, one antibody can actually access two antigens if the distance among the antigen molecules is statistically closer at higher density (antibody 'avidity'). Thirdly, a higher antigen density causes a higher probability for cross-linking the dextran matrix, which increases the viscosity of the interaction environment. In order to make a comparison with 2D matrices, a SAM with lipoic acid (LA) was employed as a $-\text{COOH}$ matrix to covalently attach mouse IgG with the same EDC/NHS chemistry. Much lower slopes were obtained for the dose-response curves of LA chips (cf. Figure 8(A) (e), (f)), even at a comparable amount of bound mouse IgG. One obvious explanation is that the metal induced fluorescence quenching is less for the dextran matrix than for the LA chip. Another possibility is the difference in the antibody's recognition efficiency between the two matrices. As one can expect, the dextran chain extends ~ 100 nm into the bulk solution, providing a nearly homogenous condition for biomolecular interaction and thus a higher interaction probability. One can speculate that it would be more difficult for the antibody to approach the epitope fixed on a flat surface due to steric hindrance issues. The source of contribution can be further clarified by comparing their dose-response curves obtained from the distance-independent responses. In any case, the fact that one can obtain dose-response curves with a much steeper slope (thus higher sensitivity) confirms the advantage of using a 3D matrix in the SPFS-based bio-affinity assays.

3.7 Observations of the 3D matrix 2-dimensionally

Surface plasmon fluorescence microscopy, or SPFM, has also been developed for spatially-resolved biosensing,²¹ which can directly meet the needs in reading out signals of DNA or protein microarrays. Based on the dextran matrix, a binding assay is conducted to investigate the principle.

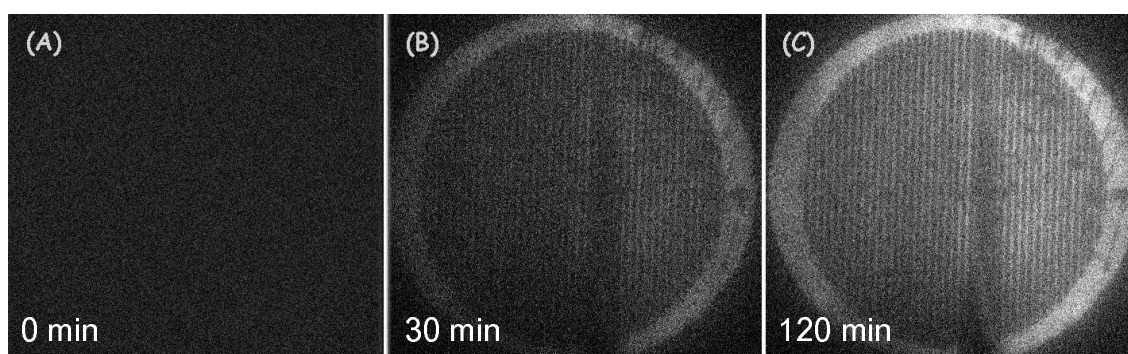
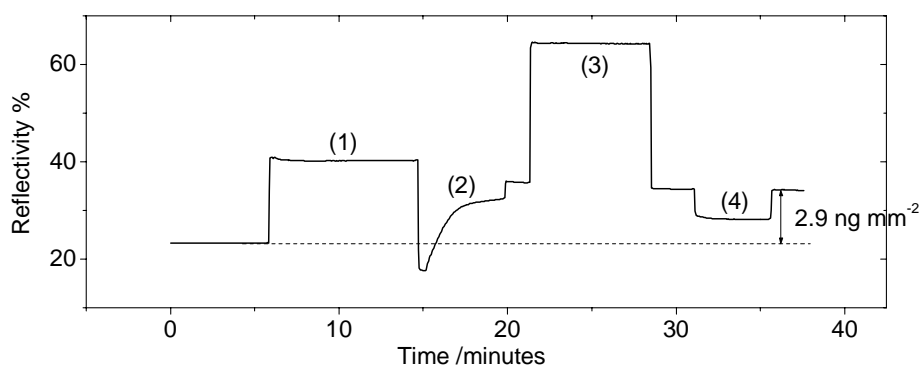


Figure 9: (Upper panel) Immobilization of mouse IgG on a dextran surface patterned by UV-lithography. Procedure (1), (2), (3) and (4) correspond to EDC/NHS activation, IgG immobilization, ethanolamine deactivation, glycine buffer regeneration (cf. Method chapter). (Lower panel) SPFM images obtained before (A) and after (B)(C) the binding of 60 pM AF-RaM to the mouse IgG immobilized dextran surface. The CCD camera was operating at $-30\text{ }^{\circ}\text{C}$, intergration time = 15 sec, bining = 2.

In order to generate the surface pattern, a dextran surface was illuminated by UV light (254 nm) through an SEM copper grid for 40 minutes. Due to the photo-ablation mechanism, the dextran layer exposed to the UV light was oxidized and removed by rinsing with copious amounts of water. The exposed area was then passivated by dipping the substrate into a 500 nM ethanol solution of the spacer thiol (cf. Table 1) for ~ 10 minutes. The remaining dextran layer was then covalently modified by a decent amount of mouse IgG, followed by the SPR response which was essentially the averaged response from both the functional and passivated areas on the patterned surface (cf. Figure 9 (A)). As a result, the average loading density of the mouse IgG was $\sim 2.9\text{ ng mm}^{-2}$. The value was $\sim 41\%$ of the density obtained on the unpatterned matrix ($\sim 7\text{ ng mm}^{-2}$), which is in agreement with the areal ratio of 39% of the copper grid. As expected, the patterned dextran layer showed no feature recorded with the cooled CCD camera at a wavelength of $670 \pm 5\text{ nm}$. (cf. (A) in Figure 9). Upon the introducing of a 60 pM AF-RaM solution, the fluorescence pattern gradually became visible within 30 minutes (cf. (B)) and the contrast was more pronounced at 120 minutes (cf. (C)). This demonstrates (1) a successful generation of the heterogeneity in the matrix by the UV-lithographic strategy, and (2) at least pico-molar sensitivity of SPFM.

4. CONCLUSIONS

Supra-molecularly-controlled interfacial architectures can be designed and experimentally realized allowing for a highly efficient recognition and binding of certain analyte systems from solution to their surface-attached complementary interaction partners (probes/targets, antigens/antibodies, ligands/receptors). Combining with a powerful tool, surface plasmon fluorescence spectroscopy, we not only are enabled to understand the nature of the interfacial molecular

arrangement, but also have realized unprecedented sensitivities in bioassays. These layers are important platforms for fundamental biophysical studies as well as for practical biosensing tasks.

5. ACKNOWLEDGEMENTS

The authors acknowledge Björn Persson, Stefan Löfås (Biacore AB, Sweden) for their supports in the work related to the dextran surface, Dr. Peter E. Nielsen (Panum Institute, Copenhagen) for sharing his experiences in PNA synthesis. Part of the DNA work was supported by an EU grant (QLKI-2000-31658, DNA-track) and by the Deutsche Forschungsgemeinschaft (KN 224/13-1).

6. REFERENCES

1. Ziegler, C., Göpel, W. *Curr. Opin. Chem. Biol.*, 2, 585-591, 1998.
2. Wegner, G. J., Wark, A. W., Lee, H. J., Codner, E., Saeki, T., Fang, S., Corn R. M., *Anal. Chem.*, 76, 5677-5684, 2004.
3. Southern, E., Mir, K., Shchepinov, M. *Nat. Biotechnol.* 21, 5-9, 1999.
4. Yu, F., Yao, D., Knoll, W. *Nucleic Acids Res.* 32, e75, 2004.
5. Malicka, J., Gryczynski, I., Gryczynski, Z., Lakowicz, J.R. *Anal. Biochem.* 315, 57-66, 2003.
6. He, L., Smith, E. A., Natan, M. J., Keating, C. D. *J. Phys. Chem. B* 108, 10973-10980, 2004.
7. Liebermann, T., Knoll, W. *Colloid Surf. A* 171, 115-130, 2000.
8. Liebermann, T., Knoll, W., Sluka, P., Herrmann, R. *Colloid Surf. A*, 169, 337-350, 2000.
9. Yu, F., Yao, D., Knoll, W. *Anal. Chem.* 75, 2610-2617, 2003.
10. Yu, F., Persson, B., Loefas, S., Knoll, W. *J. Am. Chem. Soc.* 126, 8902 -8903, 2004.
11. A. Nemetz, W. Knoll, *J. Raman Spectroscopy* 27, 587-592, 1996.
12. Roy, S., Kim, J., Kellis, J. T., Jr, Poulouse, A. J., Robertson, C. R., Gast, A. P. *Langmuir* 18, 6319-6323, 2002.
13. Barnes, W. L. *J. Mod. Optic.* 45, 661-699, 1998.
14. Vasilev, K., Knoll, W., Kreiter, M. *J. Chem. Phys.* 120, 3439-3445, 2004.
15. Stenberg, E, Persson, B., Roos, H, Urbaniczky, C. *J. Colloid Interface Sci.*, 143, 513-526, 1991.
16. Löfås, S., Johnsson, B. *J. Chem. Soc. Chem. Commun.* 21, 1526-1528, 1990.
17. Cui, X. Q., Pei, R. J., Wang, X. Z., Yang, F., Ma, Y., Dong, S. J., Yang, X. R. *Biosens. Bioelectron.*, 18, 59-67, 2003.
18. Spinke, J., Liley, M., Schmitt, F. -J., Knoll, W. *J. Chem. Phys.* 99, 7012-7019, 1993.
19. Marquart, M., Deisenhofer, J., Huber, R., Palm, W. *J. Molec. Biol.* 141, 369-391, 1980.
20. Yao, D., Yu, F., Kim, J., Nielsen, P. E., Sinner, E. -K., Knoll, W. in preparation.
21. Liebermann, T., Knoll, W. *Langmuir* 19, 1567-1572, 2003.